IJTRET International Journal of Trendy Research in Engineering and Technology
Volume 3 Issue 5 October 2019
ISSN NO 2582-0958

PREPARATION OF PURE AND AL SUBSTITUTED LANGANITE ($LA_3GA_{5.5}NB_{0.5}O_{14}$) CERAMICS AND ITS TRANSPORT PROPERTY STUDIES

N.Marimuthu, M.Rathnakumari , P. Suresh Kumar*,
[a].*Materials Research Centre, Velammal Engineering College, Chennai-600 066, Tamil Nadu, India*
**Corresponding author : suresrath@yahoo.com*

Received 16 October 2019 Received in revised form 18 October 2019 Accepted 22 October 2019
Available online 25 October 2019

ABSTRACT

Pure and Al substituted Langanite ($La_3Ga_{5.5}Nb_{0.5}O_{14}$) ceramics have been synthesized by solid state sintering method and studied their structural, dielectric and electrical properties. The crystalline nature was confirmed by powder XRD studies. The ac conductivity and dielectric properties of $La_3Ga_{5.5-x}Al_xNb_{0.5}O_{14}$ samples were examined by using complex impedance technique. Surface morphology and elemental composition were studied by energy-dispersive x-ray spectroscopy and scanning electron microscopy. The frequency dependence of dielectric constant, dielectric loss and AC conductivity were studied in the frequency range of 100 KHz to 3 MHz at different temperatures. The activation energy was calculated using Arrhenius plot. The lattice parameter, grain size, dielectric constant and AC conductivity of pure LGN ceramics were deeply affected by Al substitution in pure LGN.

1 INTRODUCTION

Piezoelectric materials are promising candidate suitable for the fabrication of functional devices such as frequency filters, sensor and high power positioning systems owing to the incomparable pairing of mechanical and electrical stimulants and their responses [1-4].

Lead free $Ca_3Ga_2Ge_40_{14}$-type structured piezoelectric single crystals are suitable piezoelectric materials for fabrication of gas sensors and combustion pressure sensors [5]. Langasite($La_3Ga_5SiO_{14}$- LGS) materials with above said structure are the most attractive piezoelectric materials for use at high temperature as it has phase stability in the wide range of temperature up to its melting point of 1470^0C [6]. The LGS type substrates demanded high electric resistivity at high temperature for real sensor applications [3]. However LGS materials show low resisitvity at high temperature.

Langanite ($La_3Ga_{5.5}Nb_{0.5}O_{14}$-LGN) is another piezoelectric material which belongs to LGS structure exhibiting a higher electromechanical coupling factors and high frequency stability than LGS. The Langanite structure is represented by a general chemical formula $A_3BC_3D_2O_{14}$ and belong to the trigonal symmetry, space group P321 and the point group 32. La^{3+}occupies the A site, octahedral positions B are occupied with equal probability of Ga^{3+} and Nb^{5+}, Ga^{3+} occupies the remaining positions (C and D) [7].

The substitution of Al in Langanite ceramics is expected to increase the resitivity of Langanite ceramics. In addition it also reduces the expensive Gallium content in the Langanite ceramics.

In certain applications, the polycrystalline material may even have advantages in composition control, homogeneity, performance, cost and ease of fabrication [8]. Though there are numerous reports on the growth of Langasite crystals, only few reports are available on the preparation of Langasite ceramics [9,10]. Seh*et al.* have reported Sr doped Langasite polycrystalline materials which has high activation energy [11]. We reported that the Al-substituted LGS ceramics shows a higher electrical resisitivity when compared to the pure LGS ceramics [12].

In this chapter synthesis of pure and Al substituted Langanite (LGN) ceramics is reported. The Langanite ceramics has been prepared by solid state reaction technique and the dielectric and impedance properties were studied.

2 EXPERIMENTAL PROCEDURE

2.1 Materials

High pure (99.99%, Sigma Aldrich) Lanthanum oxide (La_2O_3), Gallium oxide (Ga_2O_3), Niobium dioxide (Nb_2O_3) and Aluminium oxide (Al_2O_3) were used as raw materials; polyvinyl alcohol (PVA)(C_2H_4O)x was used as a binder.

2.2 Synthesis of $La_3Ga_{5.5-x}Al_xNb_{0.5}O_{14}$ Cerami

The Langanite ceramics $La_3Ga_{5.5}Nb_{0.5}O_{14}$ doped with Aluminium ($La_3Ga_{5.5-x}Al_xNb_{0.5}O_{14}$) for different mole fraction (x=0, 0.1, 0.2, 0.3 and 0.4), denoted here after LGAN synthesized by conventional solid state reaction method. Stoichiometric quantities of the starting materials were weighed and mixed in an agate mortar for 6 h, PVA used as binder and pressed into pellets of 12 mm diameter and 1 mm thickness with a hydraulic press at 2.5 MPa. After burning out of PVA, The pellets sintered at 1000°C for 10 h, further sintered at 1400°C for 2 h in air. Silver paste was painted on both surface of the disk samples and then baked at 500°C for 10 min to form the electrodes for measurement the properties of the obtained ceramics.

2.3 Characterization

The purity of the Langanite phase was checked by powder X ray diffraction using Rigaku D/max-A X-ray diffractometer with CuKα radiation in the range of $10 < 2\theta < 80$. ($\lambda = 1.5443$ nm). High Resolution Scanning Electron Microscopy was used to determine microstructure of the samples and Energy Dispersive Spectroscopy (EDS) has been employed to study the elemental composition of the samples. Transport properties like dielectric constant, the loss tangent and the AC conductivity as functions of frequency in the range of 100 Hz to 5 MHz at different temperatures were studied using Waynkerr Multi-component precision analyzer 6440B.

3.RESULTS AND DISCUSSION

3.1 Analysis of XRD Patterns

X-ray diffraction analysis was used to study the phase purity and crystalline structure of the $La_3Ga_{5.5-x}Al_xNb_{0.5}O_{14}$ (x = 0, 0.1, 0.2, 0.3 and 0.4) ceramics. XRD patterns of $La_3Ga_{5.5-x}Al_xNb_{0.5}O_{14}$ ceramics synthesized by a solid-state reaction at 1400^0Cis shown in Figure 1. In Figure 1a all the diffraction peaks in the powder XRD patterns of the LGAN ceramics were indexed by the Langasite type structure (JCPDS No: 72-2249). Other diffraction line, but with very low intensities, are identified over x>0 as belonging to β-Ga_2O_3 (denoted with stars in Figure 1). Figure 1b shows that the prominent peaks (2 -1 1) and (2 0 1) shifted towards the higher 2θ value with increasing content of Aluminium. The shift increases with the increase in Al content and corresponds to a decrease of the distances between the crystalline planes [13]. When the Al content increases the XRD data processing shows the decrease in the unit cell volume for LGAN samples which confirms that the Al is incorporated into LGN matrix without the presence of any secondary phase. Table 1 show the calculated lattice parameter values from the powder XRD spectrum and also confirms the decrease of cell volume with increasing Al content.

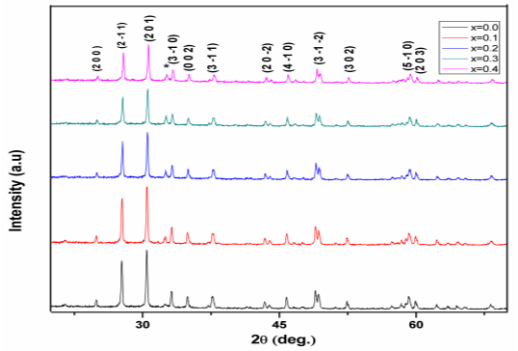

(a)

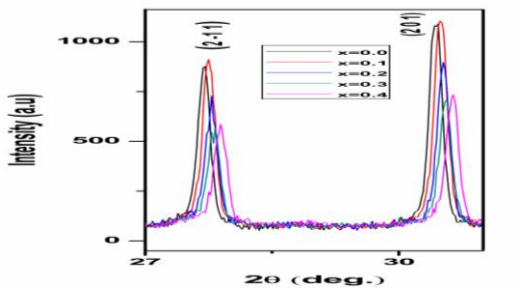

(b)

Figure 1(a) XRD pattern of $La_3Ga_{5.5-x}Al_xNb_{0.5}O_{14}$ ceramics for the composition x=0, 0.1, 0.2, 0.3 and 0.4. (b) Shows shifting peaks (2 -1 1) and (2 0 1) towards higher 2θ values

Table 1 The calculated Lattice parameter of $La_3Ga_{5.5-x}Al_xNb_{0.5}O_{14}$ ceramics

Concentration(X)	a=b (Å)	c (Å)	V (Å^3)
X=0	8.202	5.126	298.63
X=0.1	8.194	5.114	297.35
X=0.2	8.190	5.109	296.77
X=0.3	8.188	5.106	296.45
X=0.4	8.182	5.102	295.78

3.2 SEM and EDX Analysis

Scanning electron microscopic (SEM) surface photographs of $La_3Ga_{5.5-x}Al_xNb_{0.5}O_{14}$ (x = 0, 0.1, 0.2, 0.3 and 0.4) ceramics for various amounts of Al_2O_3 addition are shown in Figure 2. For all the prepared ceramics, a clear grain boundary was well established. All the grains are tightly bound pores free and hence, the ceramics possess high density which suggests that all the prepared ceramics have been well sintered. From the micrograph a uniform pseudo-hexagonal shaped with large agglomeration microstructure is observed in all the ceramics. However, the grain size increases with increasing in Al concentration. It is confirmed that the Al substitution is helpful in improving the sinterbility, due to the fact that there are some oxygen vacancies in the Al-substituted samples, making the diffusion easier [14]. The average grain size of pure and Al substituted ceramics sintered at 1400 °C are 1, 0.9, 1.2, 1.5 and 1.8 µm for Al content with x values 0.0, 0.1, 0.2, 0.3, and 0.4 respectively. The ceramics with x value of 0.4 Al substitutions have a homogeneous microstructure and well-grown grains.

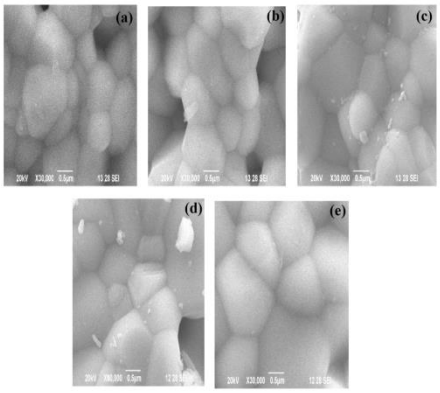

Figure 2 HRSEM pictures of $La_3Ga_{5.5-x}Al_xNb_{0.5}O_{14}$ ceramics(a) x=0 (b) x=0.1, (c) x=0.2, (d) x=0.3, (e) x=0.4

Elemental analyses through EDX were also carried out on prepared $La_3Ga_{5.5-x}Al_xNb_{0.5}O_{14}$ (x = 0, 0.1, 0.2, 0.3 and 0.4) ceramics and is shown in Figure 3. The EDX spectrum of the prepared ceramics shows that all the samples have nearly expected elemental composition and reveal the presence of La, Ga, Nb, Al and oxygen for the ceramics $La_3Ga_{5.5-x}Al_xNb_{0.5}O_{14}$ with x = 0.0 - 0.4.

Table 2 shows the measured atomic concentration of the elements present in the prepared samples . From the Table 2 it can be seen that the atomic percentage of Al increases with increasing the amount of Aluminium content.

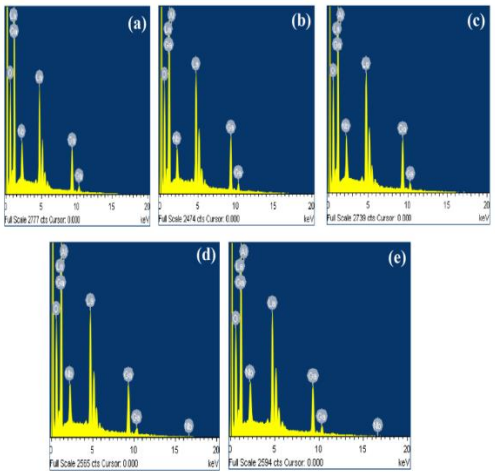

Figure 3 EDAX pictures of $La_3Ga_{5.5-x}Al_xNb_{0.5}O_{14}$ ceramics(a) x=0 (b) x=0.1, (c) x=0.2, (d) x=0.3, (e) x=0.4

Table 2 Atomic concentration of elements in $La_3Ga_{5.5-x}Al_xNb_{0.5}O_{14}$ ceramics

	Atomic % of La	Atomic % of Ga	Atomic % of Nb	Atomic % of O	Atomic % of Al
(a) X=0	11.51	21.46	3.50	63.54	0
(b) X=0.1	12.05	20.81	3.66	63.33	0.14
(c) X=0.2	12.14	20.67	3.19	63.80	0.20
(d) X=0.3	12.68	20.23	3.40	63.24	0.37
(e) X=0.4	12.33	19.90	3.37	64.07	0.41

3.3 Dielectric Studies

3.3.1 Dielectric constant

Frequency dependant dielectric constant of $La_3Ga_{5.5-x}Al_xNb_{0.5}O_{14}$ ceramics for different composition in the frequency range of 100 Hz to 5 MHz at 305 and 373 K is show in Figure 4(a-b). From Figure 4 (a-b) it is observed that the dielectric constant shows decreasing tendency with increasing in frequency.

Dielectric constant is high at low frequency which is due to the role of electronic, ionic, orientation, dipolar and space charge polarization [15]. As frequency is increased, the polarization mechanism which is having large relaxation time cease to respond to the applied field and hence the dielectric constant is decreased. The contribution from the space charge polarization is dominant at low frequencies. But it decreases slowly with increases of frequency. The space charge arises from the charge accumulation at the electrode interface and at the grain boundaries, mostly due to the vacancies of oxygen. When increase the frequency, these dipoles due to space charge do not respond to the applied electric field at high frequencies. Only the electronic polarization with large relaxation time exists and all other polarizations ceased at high frequencies [16]. Hence the net dielectric constant decreases as frequency increases. Pure LGN shows the higher dielectric constant compared to all other substituted samples. But $La_3Ga_{5.5-x}Al_xNb_{0.5}O_{14}$ (x=0.4) shows the low values of ε_r at high frequency among all the samples.

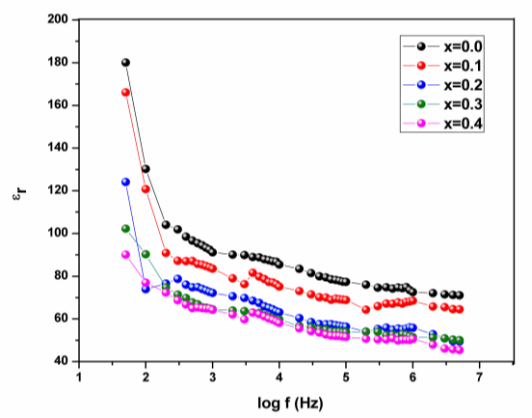

(a)

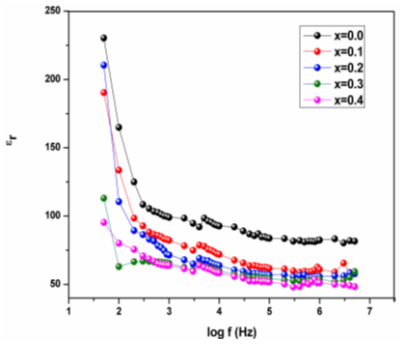

(b)

Figure 4 Frequency dependence of dielectric constant of pure and Al substituted LGN ceramics at (a) 305K and (b) 373 K

Figure 4(a) shows that the dielectric constant decreases with increasing Al substitution which is due to the fact that addition of Al^{3+} ions replace the Ga^{3+} ions on C,D and half of the B sites which is mainly responsible for both hopping exchange between the localized sites and space charge polarization[17].

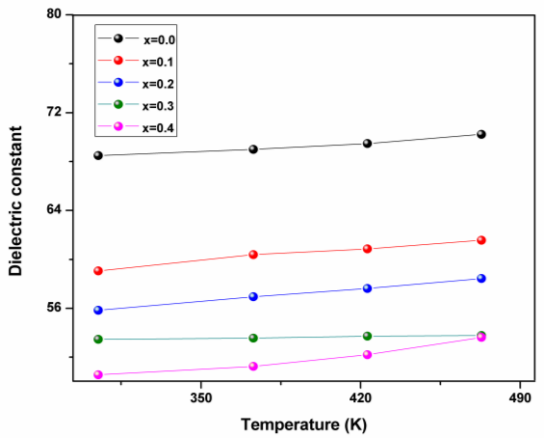

Figure 5 Temperature dependence of dielectric constant for pure and Al substituted LGN ceramics

Temperature dependence of dielectric constant of the prepared $La_3Ga_{5.5-x}Al_xNb_{0.5}O_{14}$ ceramics is shown in Figure 5. The Figure shows that the dielectric constant increases gradually as a temperature increases. This is because of availability of more space for the easy rotation of dipoles and ions, and also due to interfacial polarization which occurs in the samples. Additionally, when the temperature increases, the density of defects such as charged defects, micro-porosities and oxygen vacancies also increases which in turn increases the polarization leading to high dielectric constant at high temperature. Since the materials found to have very stable dielectric constant at higher frequency range i.e 1 KHz – 5 MHz, the prepared ceramics may be suitable for high frequency applications.

3.3.2 Dielectric Loss

Figure 6 (a-b) shows the variation of dielectric loss with frequency and temperature of LGN and LGAN samples. The dielectric loss of all the prepared ceramics shows higher values at low frequency and decreases gradually with the increasing frequency, illustrating the relaxation process. The higher value of dielectric loss at low frequency may be due to the contributions of interfacial loss and accumulation of free charge. Some amount of the electrical energy is lost in the form of heat upon electric current passes

through a sample. So, the energy loss is high at low frequency and is negligible at high frequency. The higher value of dielectric loss at lower frequencies is also due to imperfections, defects and particle size reduction. From the Figure 6 we observed that the dielectric loss increases with the increase temperature. This indicates the dielectric relaxation of the system has thermally activated nature. This kind of thermally activated nature of dielectric materials is useful for Complementary metal-oxide-semiconductor (CMOS) technology such as transistors, gate dielectrics and so on. The Figures 6 (a-b) show that the dielectric loss decreases with increasing Aluminium concentration. The decrease in dielectric loss with increase in Al concentration is due to the interfacial polarization mechanism occurring in the ceramics.

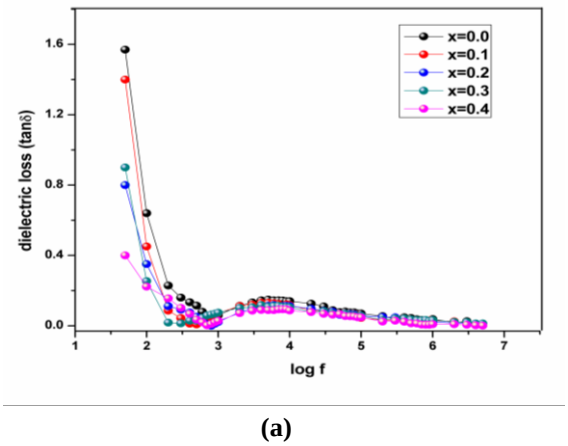

(a)

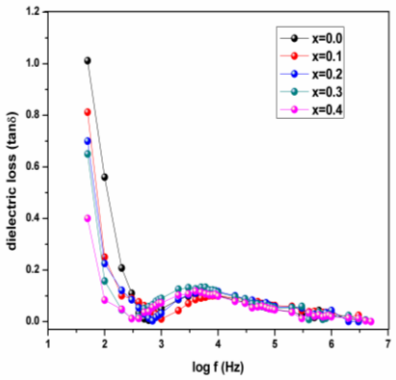

(b)

Figure 6 Frequency dependence of dielectric loss of pure and Al substituted LGN ceramics at (a) 305 K and (b) 373 K

3.3.3 AC conductivity studies

Figure 7 (a-b) shows the variation of AC conductivity (σ_{ac}) with frequency at different temperature for $La_3Ga_{5.5-x}Al_xNb_{0.5}O_{14}$ ceramics.

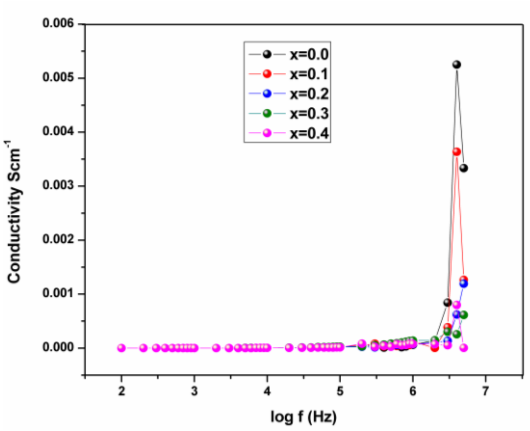

(a)

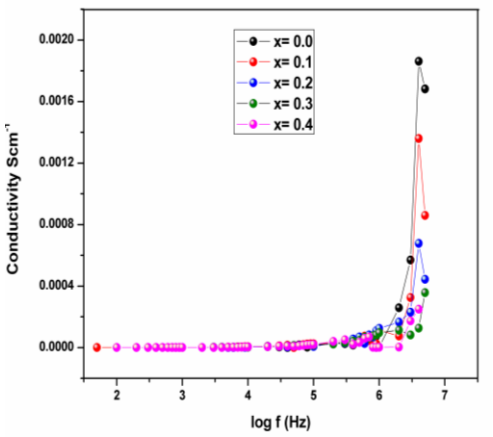

(b)

Figure 7 Variation of AC conductivity with frequency of pure and Al substituted LGN ceramics at (a) 305 K and (b) 373 K

Figure 7 shows that the magnitude of AC conductivity of all the ceramics is constant at low frequency region, and above the characteristic frequency the conductivity rapidly increases with increase in frequency. The AC conductivity value is large at high frequency region which may be due to the short-range intrawell hopping of charge carriers between localized states [18]. Pure LGN shows higher AC conductivity among all the samples. By increasing the Wt% of Al contents the electrical conductivity of $La_3Ga_{5.5-x}Al_xNb_{0.5}O_{14}$ ceramics found to decrease. This is because of the fact that increasing Aluminium concentration produces the nucleation of vacancy clustering or domains which result in decrease the number of charge carriers.

Figure 8 shows the AC conductivity log (σ_{AC}) as a function of the reciprocal temperature (1000/T) in the investigated temperature range for the pure and Al substituted $La_3Ga_{5.5-x}Al_xNb_{0.5}O_{14}$ ceramics. From the Figure 8, it is seen that AC conductivity increases linearly with the increasing temperature. This indicates that the σ_{ac} is a thermally activated process.

The mobility of free charge carriers increases with increase in temperature which in turn increases the conductivity of the material. The increase of ac conductivity for the prepared samples with increasing temperature shows the semiconducting behavior of the as-synthesized $La_3Ga_{5.5-x}Al_xNb_{0.5}O_{14}$ ceramics.

The activation energy can be calculated from the slope of the Arrhenius plot using Arrhenius equation $\sigma = \sigma_0 \exp(-E_a/kT)$. It gives the information about conduction through thermally assisted tunneling of charge carrier movement in the band tails of localized states. The obtained value of the activation energy for the samples is listed in Table 3. The table shows that the activation energy for Aluminium substituted samples at a various doping level (x = 0-0.4), increases with increasing concentration of Al ions due to the fact that Al^{3+} act as strong scatter centers and disturb the conduction path. Also as the substitution content increases, the charge localization increases which in turn reduce the concentration of hopping conducting carriers. Therefore both the activation energy and electrical resistivity increases with increase of Aluminium concentration

Table 3 AC conduction activation energies of $La_3Ga_{5.5-x}Al_xNb_{0.5}O_{14}$ ceramics

Al concentration	AC conduction activation energy (eV)
(a) X=0	0.896
(b) X=0.1	0.947
(c) X=0.2	0.954
(d) X=0.3	0.971
(e) X=0.4	1.103

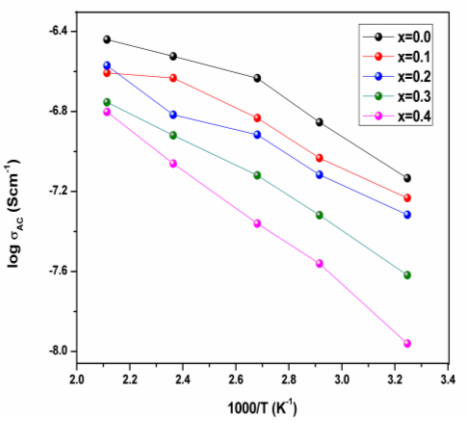

Figure 8 Variation of AC conductivity with temperature of $La_3Ga_{5.5-x}Al_xNb_{0.5}O_{14}$ ceramics

4 CONCLUSION

In this study, $La_3Ga_{5.5-x}Al_xNb_{0.5}O_{14}$ ceramics with the addition of Aluminium were prepared by solid state sintering technique. X-ray diffraction analysis indicated a pure solid solution of LGN phase with Al without any secondary phases and it shows LGS type structure. SEM micrographs of the prepared samples indicate regular, fine-grained, and almost pore-free microstructures. From the dielectric studies, it was found that the dielectric constant and loss decreased with increasing frequency but increased with temperature. It has been observed that the increase of Al content reduces the dielectric constant as well as loss. The minimum dielectric constant is observed for 0.4 wt.% of Al. The AC conductivity of the samples increased with increasing frequency and temperature. The increasing Al concentration in the samples is reduced their AC conductivity. The resistivity of the prepared ceramics is increased with increasing Al concentration which could be ideal for sensor applications.

References

1. Jorgen Rodel, Wook Jo, Klaus, Seifert, TP, Eva-MariaAnton, TorstenGranzow, Damjanovic 2009, 'Perspective on the development of lead-free piezo ceramics', J.Am.Ceram.soc., vol.92, no.6, pp. 1153–1177.
2. Haertling, GH 1999, 'Ferroelectric ceramics: history and technology', J.Am. Ceram. Soc., vol.82, no.4, pp. 797–818.

3. Fritze, H, Tuller, HL, Seh, H &Borchardt, G 2001, 'High temperature nanobalance sensor based on langasite', Sens. Actuators B, vol. 76, no.1-3, pp. 103–107.
4. Fritze, H &Tuller, HL 2001 'Langasite for High-Temperature Bulk Acoustic Wave Applications', Appl. Phys. Lett., vol.78, no.7, pp. 976-977
5. Kuze, T, Takeda, H Nishida, T, Uchiyama, H &Shiosaki, T 2016, 'Synthesis and Electric Properties of Alminum Substituted Langasite-type $La_3Nb_{0.5}Ga_{5.5}0_{14}$ Single Crystals', IEEE Transactions on Ultrasonics, Ferroelectrics, and Frequency Control, vol.63, no.3, pp. 486 – 505
6. Hiroaki Takeda, Satoshi Tanaka, Hiroyuki Shimizu, Takashi Nishida & Tadashi Shiosaki 2006, 'Growth and Electric Properties of Al-substituted Langasite-type $La_3Ta_{0.5}Ga_{5.5}O_{14}$ Crystals at High Temperature', Key Engineering Materials, vol. 320, pp. 239-242
7. Georgescu, S, Voiculescu, AM, Toma, O, Gheorghe, L, Achim, A, Matei, C &Hau, S 2010, 'Luminescence efficiency of Europium-doped LGS, LGT and LGN crystals', Optoelectronics and advanced materials – Rapid Communications', vol. 4, no. 12, pp. 1937 – 1941
8. Mezeix, L & Green, DJ 2006, 'Comparison of the mechanical properties of single crystal and polycrystalline yttrium aluminum garnet', Int. J. Appl. Ceram. Technol., vol.3, no.2, pp. 166–176
9. HuankiatSeh, Harry L. Tuller&HolgerFritze 2003, 'Langasite for high-temperature acoustic wave gas sensor', Sensors and Actuators B, vol.93, no.1, pp. 169–174.
10. Bakiz, Quzaouit, K, Benlhachemi, A, Gavarri, JR, Villain, S, Essoumhi, A &Benyaich, H 2008, 'Multiphase Lanthanum hydroxycarbonates and Langasite ceramics for GAS sensor', Phys. Chem. News, vol.41,pp. 55-60.
11. Seh, H, Tuller, HL, Fritze, H 2004, 'Defect properties of langasite and effects on BAW gas sensor performance at high temperatures', J. Eur. Ceram. Soc. vol.24, pp. 1425–1429.
12. Marimuthu, N, Parasuraman, R, Rathnakumari, M. Suresh Kumar, P, &Upadhyay, R.B 2018, 'Synthesis and transport properties of Al substituted langasite ceramics, Journal of Materials Science- Materials in Electronics, vol. 29, no. 2, pp. 1280-1288
13. Marimuthu, N, Rathnakumari, M. Suresh Kumar, P, &Upadhyay, R.B 2019, "Dual photoluminescence emission of Er^{3+}, Yb^{3+} and Er^{3+}/Yb^{3+} doped $La_3Ga_{5.5}Nb_{0.5}O_{14}$ ceramics under UV and IR excitation" Journal of Materials Science- Materials in Electronics, DOI: 10.1007/s10854-019-02092-4
14. LouanesHamzioui, Fares Kahoul,Boutarfaia Ahmed 2015, The Effect of Nb2O5 Addition on the Structural, Dielectric and Piezoelectric Properties of Pb0,98 Ba0,02 [(Zr0.52Ti0.48)0,98(Cr3+0.5, Ta5+0.5)0,02] Ceramics, Energy Procedia 74:198-204
15. Ashok, A, Somaiah, T, Ravinder, D, Venkateshwarlu, C, Reddy, C, Rao, K & Prasad M 2012, 'Electrical properties of cadmium substitution in nickel ferrites', World J. Condens. Matter Phys., vol.2, no.4, pp. 257–266
16. TamizhSelvi, K, Alamelumangai, K, Priya, M, Suresh Kumar, P, Rathnakumari, M 2016, 'Structural, electrical and magnetic properties of Mn_3O_4/MgOnanocomposite', J Mater Sci: Mater Electron, vol.28, no.3, pp. 2317-2324
17. Raghavender, AT &Jadhav, KM, 2009, 'Dielectric properties of Al-substituted Co ferrite nanoparticles', Bull. Mater. Sci., vol.32, no.6, pp. 575–578
18. Abdul Gafoor, AK, Musthafa, MM &Pradyumnan, PP 2012, 'Effect of Nd^{3+} Doping on Optical and Dielectric Properties of TiO_2 Nanoparticles Synthesized by a Low Temperature Hydrothermal Method', Jr. of Nano Science and Nano Technology, vol.1, no.2, pp. 53-57